Vol 16 No 8, August 2007
1009-1963/2007/16(08)/2296-08

Chinese Physics

© 2007 Chin. Phys. Soc.
and IOP Publishing Ltd

Density functional theory for molecular orientation of hard rod fluids in hard slits*

Cao Da-Peng(曹达鹏)†, Cheng Li-Sheng(程礼盛), and Wang Wen-Chuan (汪文川)

Division of Molecular and Materials Simulation, Key Laboratory of Nanomaterials, Ministry of Education Beijing University of Chemical Technology, Beijing 100029, *China*

(Received 10 January 2007; revised manuscript received 1 March 2007)

A density functional theory (DFT) is used to investigate molecular orientation of hard rod fluids in a hard slit. The DFT approach combines a modified fundamental measure theory (MFMT) for excluded-volume effect with the first order thermodynamics perturbation theory for chain connectivity. In the DFT approach, the intra-molecular bonding orientation function is introduced. We consider the effects of molecular length (i.e. aspect ratio of rod) and packing fraction on the orientations of hard rod fluids and flexible chains. For the flexible chains, the chain length has no significant effect while the packing fraction shows slight effect on the molecular orientation distribution. In contrast, for the hard rod fluids, the chain length determines the molecular orientation distribution, while the packing fraction has no significant effect on the molecular orientation distribution. By making a comparison between molecular orientations of the flexible chain and the hard rod fluid, we find that the molecular stiffness distinctly affects the molecular orientation. In addition, partitioning coefficient indicates that the longer rodlike molecule is more difficult to enter the confined phase, especially at low bulk packing fractions.

Keywords: density functional theory, rodlike chain, molecular orientation, flexible chain
PACC: 0570C, 6120G, 6125E

1. Introduction

Nonspherical particles, say rodlike molecules and platelet molecules, are described by versatile model systems to explore a wide range of phenomena in colloidal and polymer sciences as well as condensed matter ranging from fluid phase separations to the emergence of a nematic ordering structure.[1,2] As a prototype of the liquid crystals, the rodlike molecule model has been extensively applied to the investigation of the nematic-isotropic phase transition of the liquid crystals via the molecular simulation and density functional theory.[3] Recently, by exploring the binary mixtures of the hard rod-sphere,[4−6] rod-platelet,[1,7] investigators have found that the rodlike fluids can also act as a shield to stabilize a solution or as an additive to induce the colloids into self-assembly,[8−11] which is similar to the properties of a flexible polymeric stabilizer.[12]

Since a modified fundamental measure theory (MFMT)-based DFT method was proposed by Yu and Wu [13] and Roth *et al*[14] separately, it has been widely employed to explore the properties of different polymer systems,[15] including the microstructures of flexible polymer fluids,[16−20] surface forces between polymer brushes[12,21] and adsorption and phase behaviour of polymer fluids in model pores.[22−28] All these calculations suggest that the MFMT-based DFT approach can excellently reproduce the microstructures and thermodynamic properties of polymer fluids by comparison with these data from Monte Carlo simulations. However, few reports are available for the application of MFMT-based DFT to the rodlike molecules. In our previous work, although we used a hybrid DFT to investigate the self-assembly of rodlike molecules, the hybrid DFT must resort to the single-chain Monte Carlo simulation as an input for solving the ideal-gas part of Helmholtz energy of the rodlike fluids,[19] while in this work, we derive the analytical expression on the ideal-gas part of Helmholtz energy for the rodlike molecule, which can patch up the disadvantage that the hybrid DFT needs single-chain Monte Carlo simulation as an input. In addition, we introduce the intra-molecular bonding orientation correlation function into the MFMT-based DFT. The MFMT-based DFT is therefore valid for the calcula-

*Project supported by the National Natural Science Foundation of China (Grant No 20646001), the Beijing Novel Program (Grant No 2006B17), the Program for New Century Excellent Talents in University (NCET), the "Chemical Grid Program" and the Excellent Talent Fund of Beijing University of Chemical Technology.
†E-mail:caodp@mail.buct.edu.cn and cao_dp@hotmail.com

tion of the molecular orientation of the rodlike and flexible chains. From a theoretical point of view, the present DFT is in a perfect self-consistent framework.

The rest of this paper is organized as follows. First, we briefly describe the DFT theory for hard rod fluids, including a model of the hard rod, the Helmholtz energy functional, and the analytical expression for the density profiles of the hard rods in hard slit. Second, the introduction of intra-molecular bonding orientation correlation function is presented. Then, we investigate the effects of chain length and packing fraction on molecular orientations of the hard rod fluids and the flexible polymer fluids. Finally, some discussion is given.

2. Theory for hard rod fluids

2.1. Model of hard rod fluid

In this work, the hard rod fluid is modelled as a tangentially connected hard sphere chain where the bond length is equal to the segment diameter σ, and the bond angle is fixed at $\theta_0 = \pi$.

In general, the bonding potential for a tangentially connected hard sphere chain can be expressed as[29]

$$V_{\mathrm{B}}(\boldsymbol{R}) = \sum_{i=1}^{M-1} V_{\mathrm{BL}}(|\boldsymbol{r}_{i+1} - \boldsymbol{r}_i|) + \sum_{i=2}^{M-1} V_{\mathrm{BA}}(\theta_{i-1,i,i+1}), \quad (1)$$

where M denotes the number of segments for each chain, $\boldsymbol{R}$ is a set of coordinates describing the segmental positions, and $\theta_{i-1,i,i+1}$ is the bonding angle formed by three consecutive segments indexed by $i-1, i$, and $i+1$. For the hard rod fluids, the intramolecular Boltzmann factor satisfies

$$\exp(-\beta V_{\mathrm{B}}(\boldsymbol{R})) \propto \prod_{i=1}^{M-1} \delta(|\boldsymbol{r}_{i+1} - \boldsymbol{r}_i| - \sigma) \times \prod_{i=2}^{M-1} \delta(\theta_{i-1,i,i+1} - \pi), \quad (2)$$

where $\beta = 1/kT$ and $\delta(r)$ is the Dirac delta function. Equation (2) indicates that the probability density of a hard rod fluid with a configuration $\boldsymbol{R}$ is proportional to the Boltzmann factor $\exp(-\beta V_{\mathrm{B}}(\boldsymbol{R}))$.

2.2. Helmholtz free energy functional

The Helmholtz energy functional $F[\rho_M(\boldsymbol{R})]$ is conventionally divided into an ideal contribution from the system containing ideal chains that interact only through bonding potentials and an excess part taking into account the contributions from both non-bonded inter- and intra- molecular interactions[16]

$$F[\rho_M(\boldsymbol{R})] = F_{\mathrm{id}}[\rho_M(\boldsymbol{R})] + F_{\mathrm{ex}}[\rho(\boldsymbol{r})], \quad (3)$$

where $\rho_M(\boldsymbol{R})$ is the multi-dimensional density profile depending on the positions of all segments of the polymeric molecule. The molecular density profile $\rho_M(\boldsymbol{R})$ is related to the segmental density by

$$\rho(\boldsymbol{r}) = \sum_{i=1}^{M} \rho_{\mathrm{s}i}(\boldsymbol{r}) = \sum_{i=1}^{M} \int \mathrm{d}\boldsymbol{R}\delta(\boldsymbol{r} - \boldsymbol{r}_i)\rho_M(\boldsymbol{R}), \quad (4)$$

where $\rho(\boldsymbol{r})$ is the total segmental density and $\rho_{\mathrm{s}i}(\boldsymbol{r})$ is the local density of segment i. For polymers with only bonding potentials, the ideal Helmholtz energy is given exactly as

$$\beta F_{\mathrm{id}}[\rho_M(\boldsymbol{R})] = \int \mathrm{d}\boldsymbol{R}\rho_M(\boldsymbol{R})[\ln \rho_M(\boldsymbol{R}) - 1] + \beta \int \mathrm{d}\boldsymbol{R}\rho_M(\boldsymbol{R})V_{\mathrm{B}}(\boldsymbol{R}). \quad (5)$$

The excess part of the Helmholtz energy functional is closely related to the non-bonded intersegmental interactions and the effect of chain connectivity on inter-segmental correlations. Following by our previous work,[16,29] the excess Helmholtz energy functional is represented by

$$\beta F_{\mathrm{ex}}[\rho(\boldsymbol{r})] = \int \mathrm{d}\boldsymbol{r}\{\phi^{\mathrm{hs}}[n_\alpha(\boldsymbol{r})] + \phi^{\mathrm{chain}}[n_\alpha(\boldsymbol{r})]\}, \quad (6)$$

where $\phi^{\mathrm{hs}}[n_\alpha(\boldsymbol{r})]$ and $\phi^{\mathrm{chain}}[n_\alpha(\boldsymbol{r})]$ are the excess Helmholtz free energy densities due to hard-sphere repulsion and the effect of the chain connectivity on the inter-segmental correlations, and $n_\alpha(\boldsymbol{r})$ with $\alpha = 0, 1, 2, 3, V_1, V_2$ are Rosenfeld's weighted densities. These scalar and vector weighted densities are given by

$$n_\alpha(\boldsymbol{r}) = \sum_j n_{\alpha j}(\boldsymbol{r}) = \sum_j \int \rho_j(\boldsymbol{r}')\omega_j^\alpha(\boldsymbol{r} - \boldsymbol{r}')\mathrm{d}\boldsymbol{r}', \quad (7)$$

where $\omega_j^\alpha(\alpha = 0,\ 1,\ 2,\ 3,\ V_1,\ V_2)$ are six weight functions.[30]

According to the modified fundamental measure theory,[13,14] the excess Helmholtz energy density due to the hard-sphere repulsion includes a scalar part and a vector part, which is expressed as

$$\phi^{\rm hs}[n_\alpha(\boldsymbol{r})] = \phi^{{\rm hs}(S)}[n_\alpha(\boldsymbol{r})] + \phi^{{\rm hs}(V)}[n_\alpha(\boldsymbol{r})] = \int {\rm d}\boldsymbol{r}\Bigg\{ - n_0 \ln(1-n_3) + \frac{n_1 n_2 - \boldsymbol{n}_{V_1}\cdot\boldsymbol{n}_{V_2}}{1-n_3} + (n_2^3/3 - n_2 \boldsymbol{n}_{V_2}\cdot\boldsymbol{n}_{V_2})\left[\frac{\ln(1-n_3)}{12\pi n_3^2} + \frac{1}{12\pi n_3(1-n_3)^2}\right]\Bigg\}. \quad (8)$$

An extension of Wertheim's first-order perturbation theory for the chain connectivity to inhomogeneous systems gives[13,29]

$$\phi^{\rm chain}(n_\alpha) = \frac{1-M}{M} n_0 \cdot \xi \cdot \ln y^{\rm hs}(\sigma, n_\alpha), \quad (9)$$

where $\xi = 1 - \boldsymbol{n}_{V_2}\cdot\boldsymbol{n}_{V_2}/n_2^2$ denotes the inhomogeneous factor, and $y^{\rm hs}(\sigma, n_\alpha)$ is the contact value of the cavity correlation function between segments, given by

$$y^{\rm hs}(\sigma, n_\alpha) = \frac{1}{1-n_3} + \frac{n_2\xi\sigma}{4(1-n_3)^2} + \frac{n_2^2\xi\sigma}{72(1-n_3)^3}. \quad (10)$$

The key idea of a density functional theory is that if a grand potential functional $\Omega[\rho_M(\boldsymbol{R})]$ is given, the equilibrium density profile, $\rho_M(\boldsymbol{R})$, can be solved from the stationary condition

$$\frac{\delta\Omega[\rho_M(\boldsymbol{R})]}{\delta\rho_M(\boldsymbol{R})} = 0. \quad (11)$$

Thereby all thermodynamic properties can be evaluated by following statistical thermodynamic relations. For a polymeric fluid, the grand potential is related to the Helmholtz energy functional via the Legendre transform

$$\Omega[\rho_M(\boldsymbol{R})] = F[\rho_M(\boldsymbol{R})] + \int [\psi_M(\boldsymbol{R}) - \mu_M]\rho_M(\boldsymbol{R}){\rm d}\boldsymbol{R}, \quad (12)$$

where μ_M is the chemical potential of the polymer chain, and $\psi_M(\boldsymbol{R})$ is the external potential exerting on individual segments.

2.3. Euler–Lagrange equations

Minimization of the grand potential with respect to the density profiles, namely, Eqs.(11) and (12), yields the Euler-Lagrange equation

$$\rho_M(\boldsymbol{R}) = \exp[\beta\mu_M - \beta V_{\rm B}(\boldsymbol{R}) - \beta\sum_{i=1}^{M}\lambda_i(\boldsymbol{r}_i)], \quad (13)$$

where the self-consistent potential $\lambda_i(\boldsymbol{r}_i)$ is a summation of the functional derivative of the excess Helmholtz free energy with respect to density profiles and external potential $\varphi_i(\boldsymbol{r}_i)$,

$$\lambda_i(\boldsymbol{r}_i) = \frac{\delta F_{\rm ex}}{\delta\rho(\boldsymbol{r}_i)} + \varphi_i(\boldsymbol{r}_i). \quad (14)$$

Combination of Eqs.(4), (11) and (12) yields the segmental densities $\rho_{{\rm s}i}(\boldsymbol{r})$

$$\rho_{\rm si}(\boldsymbol{r}) = \int {\rm d}\boldsymbol{R}\delta(\boldsymbol{r}-\boldsymbol{r}_i)\exp[\beta\mu_M - \beta V_{\rm B}(\boldsymbol{R}) - \beta\sum_{j=1}^{M}\lambda_j(\boldsymbol{r}_j)]. \quad (15)$$

Accordingly, the average segment density of the hard rod chains is represented by

$$\rho(\boldsymbol{r}) = \exp(\beta\mu_M)\int {\rm d}\boldsymbol{R}\sum_{i=1}^{M}\delta(\boldsymbol{r}-\boldsymbol{r}_i) \times \exp\left[-\beta V_{\rm B}(\boldsymbol{R}) - \beta\sum_{j=1}^{M}\lambda_j(\boldsymbol{r}_j)\right]. \quad (16)$$

2.4. Density profiles of hard rod in slit pores

For hard rods in a hard slit, the external potential for each segment is given by

$$\varphi_i(z) = \begin{cases} \infty, & z<0 \text{ or } z>H, \\ 0, & \text{otherwise}, \end{cases} \quad (17)$$

where z is the perpendicular distance from the wall, and H is the pore width. For systems with the density distribution changing only in the z-direction, $\rho_i(\boldsymbol{r})$ becomes $\rho_i(z)$.[29] Thus, density profiles of segment i in a slit geometry can be derived from Eqs.(2) and (15)

$$\rho_{{\rm s}i}(z_i) = \frac{\exp(\beta\mu_M)}{2\sigma}\int_{z_i-\sigma}^{z_i+\sigma}\exp[-\beta\lambda(z_{i+1})] \cdot G_{\rm L}(z_i, z_{i+1})\cdot G_{\rm R}(z_i, z_{i+1}){\rm d}z_{i+1}, \quad (18)$$

where $G_{\rm L}(z_i, z_{i+1})$ and $G_{\rm R}(z_i, z_{i+1})$ respectively are the left and right self-recursive functions, given by

$$G_{\mathrm{L}}(z_i, z_{i+1}) = \begin{cases} 1, & i = 1, \\ \exp[-\beta\lambda(2z_i - z_{i+1})]G_{\mathrm{L}}(z_{i-1}, z_i), & i \geq 2, \end{cases} \tag{19}$$

$$G_{\mathrm{R}}(z_i, z_{i+1}) = \begin{cases} 1, & i = M-1, \\ \exp[-\beta\lambda(2z_{i+1} - z_i)]\}G_{\mathrm{R}}(z_{i+1}, z_{i+2}), & i < M-1. \end{cases} \tag{20}$$

Note that the left and right self-recursive functions are entirely different from the recurrence functions for flexible polymers. For hard rod fluids, segment i is closely related to the position of the neighbour segment. Once the position of the neighbour segment is fixed, the configuration of the hard rod fluid is known due to its special rod geometry. Compared with the recurrence functions for flexible polymers, Eqs.(19) and (20) seem to be more simple, because Eqs.(19) and (20) do not need the numerical integral. However, Eqs.(19) and (20) are the self-recursive functions rather than the recurrence functions. Obviously, Eqs.(19) and (20) are faster in computation than the expressions for semi-flexible polymers, because the computing time for the semi-flexible polymer increases exponentially rather than linearly with the increase of the chain length M.[29]

2.5. Orientation of the rod molecule

To obtain the local information on the molecular orientation of the rod or flexible polymeric chains, we introduce a set of intra-molecular distribution functions (IMDF) into the present theory.[31] The IMDF is described as

$$\rho_{i,i+1}(\boldsymbol{r}, \boldsymbol{r}') = \int \mathrm{d}\boldsymbol{R}\delta(\boldsymbol{r} - \boldsymbol{r}_i)\delta(\boldsymbol{r}' - \boldsymbol{r}_{i+1})\rho_M(\boldsymbol{R}). \tag{21}$$

In particular, for the system studied, the IMDF can be derived analytically as

$$\rho_{i,i+1}(z, z') = \frac{\theta(\sigma - |z - z'|)}{2\sigma} \exp(\beta\mu_M - \beta\lambda_i(z) - \beta\lambda_{i+1}(z'))G^i_{\mathrm{L}}(z, z')G^i_{\mathrm{R}}(z, z'). \tag{22}$$

Therefore, the bonding orientation correlation function, $\cos\omega$, can be expressed as a function of IMDF, given by

$$\langle\cos\omega\rangle = \frac{1}{M-1}\sum_{i=1}^{M-1} \frac{\int_{-1}^{1} \mathrm{d}y\rho_{i,i+1}(z - 0.5y\sigma, z + 0.5y\sigma)y^2}{\int_{-1}^{1} \mathrm{d}y\rho_{i,i+1}(z - 0.5y\sigma, z + 0.5y\sigma)}, \tag{23}$$

where $y = \cos\omega$. ω is the polar angle between the normal direction of the surface and the bond vector formed by two adjacent segments of a chain, and $\langle\ \rangle$ indicates the average of all bonding orientations of all configurations.

Finally, the orientation distribution of the rod molecules or flexible polymeric chains can be defined as

$$s(z) = \frac{3\langle\cos\omega\rangle - 1}{2}, \tag{24}$$

where z is the distance in the z direction. Therefore, it is well known that $s(z)$=1 suggests that the orientation of the rod molecule is perpendicular to the surface, $s(z)$=0 means random orientation of the rod molecule, $s(z) = -0.5$ corresponds to the parallel orientation of the rod molecule to the surface.

3. Results and discussion

We first consider the effect of molecular length on the density profiles and molecular orientation distributions of the hard rod fluids. Figures 1 and 2 show the density profiles and molecular orientation distri-

bution of the hard rod fluids in a slit of $H = 20\sigma$ at a packing fraction of $\eta = 0.1$. It is well known that the local density profiles of the confined fluids are dependent on two factors. One is the depletion effect and the other is the packing effect. The two factors often are in a competition for determining the local density of the confined fluids. It can be found from Fig.1 that at $M = 8$, the density profile near the wall is clearly smaller than the bulk density. That is to say, the depletion effect determines the local density profiles in the case. It is due to the fact that the presence of the wall causes the loss of configurational entropy of the hard rod fluids. However, with the increase of the molecular length, at $M = 16$, the depletion effect disappears. In contrast, the packing effect determines the local density profiles, which can be reflected by the higher contact density near the wall than the bulk density. When the molecular length increases to $M = 32$ and 64, the packing effect becomes clear obviously.

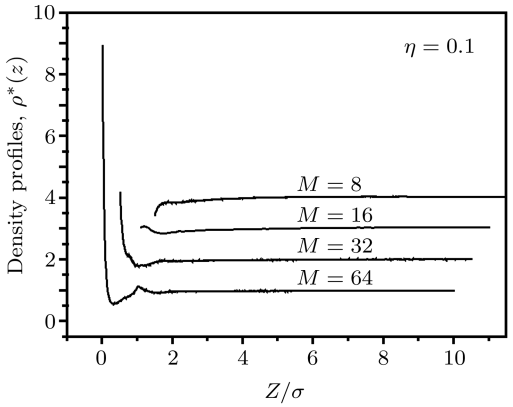


Fig.1. Density profiles of hard rod fluids in a hard slit of $H = 20\sigma$ at a packing fraction $\eta = 0.1$. Form top to bottom, the chain lengths (i.e. aspect ratio) of the hard rod are $M = 8$, 16, 32 and 64, respectively. The curves corresponding to $M = 8$, 16 and 32 have shifts of 3, 2 and 1 units upwards and 1.5, 1.0 and 0.5 units rightwards, respectively.

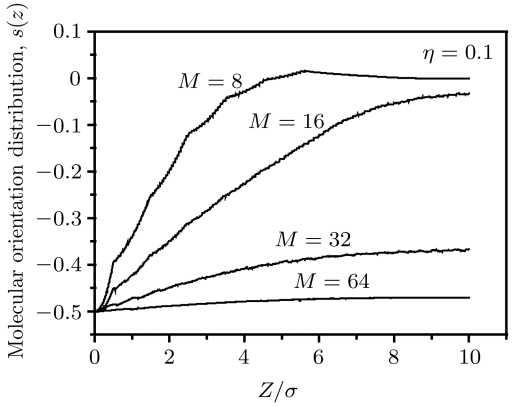


Fig.2. Molecular orientation distributions of hard rods in a hard slit of $H = 20\sigma$ at a packing fraction $\eta = 0.1$.

We can observe from Fig.2 that when the molecular mass centre of the hard rod is near the wall, the molecular orientation factor is equal to -0.5, which means that the molecular orientation of the hard rod is always parallel to the wall. With the molecular mass centre of the hard rod departing from the wall, the orientation of the rod molecules of $M = 8$ changes gradually from parallel to random. The rod molecules of $M = 16$ exhibit the same behaviour as that of $M = 8$. However, for the rod molecules of $M = 64$ and 32, their molecular orientation factors are in the range of $-0.4 - -0.5$, suggesting that the rod molecules basically remain the orientation parallel to the wall. The calculated results are in excellent agreement with the fact that the rod molecules of $M = 64$ and 32 enter the slit only by the orientation parallel to the wall because the molecule is larger than the width of the slit. To consider the effect of molecular stiffness on the orientation of chains, we also need to calculate the molecular orientation distribution of flexible chains in the slit at $\eta = 0.1$. The calculated results are shown in Fig.3. Interestingly, for the flexible chains, we observe that the chain length has no significant effect on the molecular orientation. For chain lengths of $M = 16$, 32 and 64, the molecular orientation of the flexible chain remains the same basically, while that of the hard rod is distinctly different. That is to say, the molecular stiffness is a key factor of affecting the orientation of hard chains.

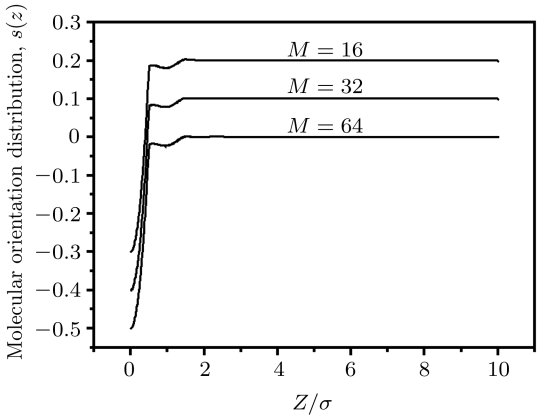


Fig.3. Molecular orientation distributions of flexible chains in a hard slit at $\eta = 0.1$. The curves corresponding to $M = 16$ and 32 have shifts of 0.2 and 0.1 units upwards, respectively.

Because the packing fraction has a significant effect on the density profiles of the hard rods, we intend to explore the behaviour of the hard rods at a high packing fraction. Figures 4 and 5 present the density profiles and molecular orientation distribution of

the hard rod fluids at $\eta = 0.2$, with the other conditions being the same as those in Fig.1. As expected, no depletion effect appears. In contrast, the density profiles for all these cases studied present the packing effect. It is noted that the contact density of rod molecule of $M = 32$ is 14 times the bulk density. Furthermore, the second peak also appears, meaning that the rod molecules have formed a thin film parallel to the wall. To obtain more clear evidences, we pay our attention to Fig.5. The molecular orientation distribution in Fig.5 shows that $s(z)$ is approximately equal to -0.5 within $z/\sigma = 0 - 1$, suggesting that the hard rod molecules flatly lie on the wall. It is also a good evidence for the formation of the thin film parallel to the wall.

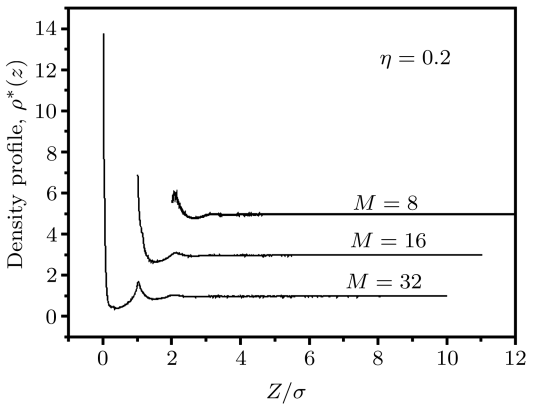


Fig.4. Density profiles of hard rod fluids at a packing fraction $\eta = 0.2$ and other conditions are the same as those in Fig.1. The curves corresponding to $M = 8$ and 16 have shifts of 4 and 2 units upwards, and 2 and 1 units rightwards, respectively.

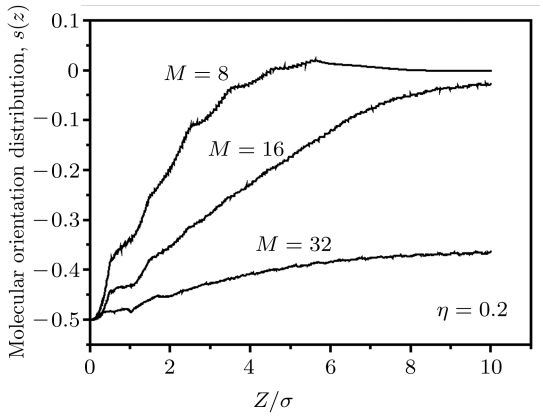


Fig.5. Molecular orientation distributions of hard rods in a hard slit at $\eta = 0.2$.

Comparing with Fig.2, we interestingly found that molecular orientation distributions basically remain the same for the hard rods with a fixed molecular length, although the packing fractions are distinctly different between Figs.2 and 5. The observations motivate us to investigate the effect of packing fraction on microstructure and molecular orientation.

Figures 6 and 7 show the density profiles and molecular orientation of the hard rod at $M = 16$ and different packing fractions.

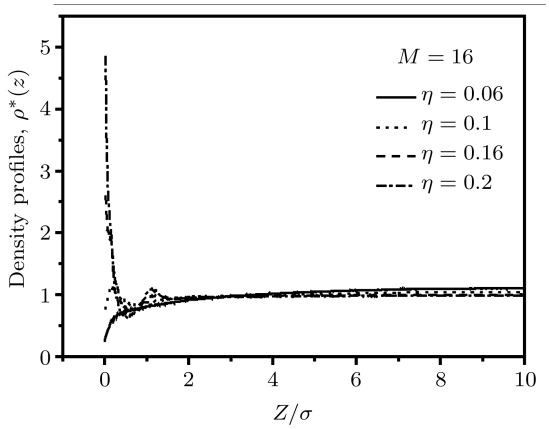


Fig.6. Density profiles of hard rod of $M = 16$ at different packing fractions in a slit.

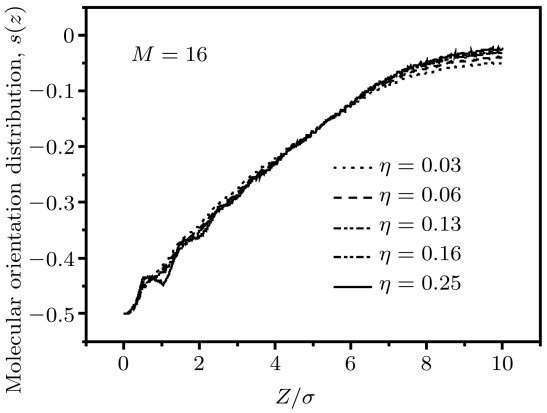


Fig.7. Effect of packing fraction on molecular orientation distribution of the hard rod fluids.

It can be found from Fig.6 that the contact value of the local densities increases with packing fraction. Furthermore, at $\eta = 0.06$, the distinct depletion effect appears, which is similar to the behaviour of flexible chains. Interestingly, the molecular orientation of the hard rods remains unchanged basically, although the packing fraction η increases from 0.03 to 0.25. That is to say, the packing fraction has no significant effect on the molecular orientation of the hard rods. To compare with the flexible chains, we also explore the dependence of molecular orientation of the flexible chain on packing fraction at $M = 16$ as shown in Fig.8. Surprisingly, the molecular orientation of the flexible

chain shows a peak in the range of $z/\sigma = 0.5 - 2$ at high packing fractions, say, $\eta = 0.25$. However, at low packing fractions, the peak of the molecular orientation distribution disappears. The observation is different from the behaviour of the hard rods, because the packing fraction has a significant effect on the molecular orientation of the flexible chains.

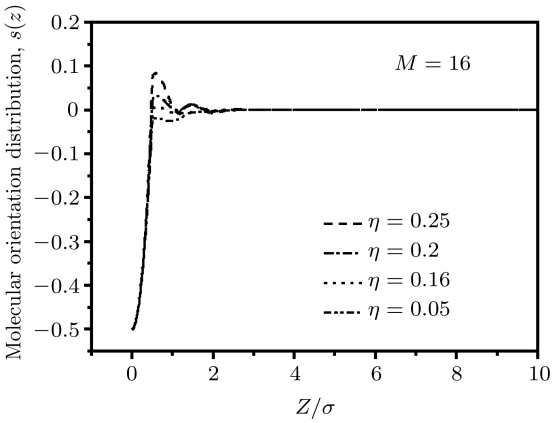


Fig.8. Effect of packing fraction on molecular orientation distribution of the flexible chains.

The hard rod molecules would lose their configurational entropy when they enter the slit. So the packing fraction of the hard rod molecule in a confined phase could be different from that in a bulk phase. We use the partitioning coefficient to represent the difference.[19] Figure 9 shows the partitioning coefficient of the hard rods changing with the bulk packing fraction, where the partitioning coefficient is defined as the molecular density in slit, divided by the bulk density.

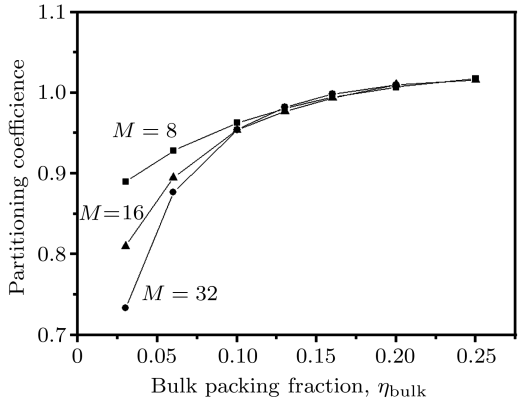


Fig.9. Partitioning coefficient as a function of bulk packing fraction for the hard rod fluids.

Interestingly, at a bulk packing fraction $\eta < 0.12$, the longer the hard rod is, the smaller the partitioning coefficient will be. However, at a bulk packing fraction $\eta > 0.12$, the length of hard rod has no significant effect on the partitioning coefficient. The reason may be that at lower bulk packing fractions, the depletion effect causes the difficulty for the long hard rod to enter the confined phase; while at high bulk packing fractions, the depletion effect disappears, leading to that the length of the hard rod has no significant effect on the partitioning coefficient.

4. Conclusions

The molecular orientation of the hard rod fluids in a hard slit has been investigated by a DFT approach, which combines the modified fundamental measure theory for the excluded-volume effect with the first order thermodynamics perturbation theory for the chain connectivity. In the DFT approach, the ideal-gas part of Helmholtz energy of the rodlike fluids is solved analytically, without any requirement for single chain Monte Carlo simulation as an input. Furthermore, the intra-molecular bond orientation function is introduced into the DFT approach. Accordingly, the MFMT-based DFT can be used to investigate the molecular orientations of the hard rod fluids and flexible polymeric chains. We consider the effects of the molecular length and packing fraction on the orientation of the hard rod and flexible chains. For the flexible chains, the chain length has no significant effect while the packing fraction shows slight effect on the molecular orientation distribution. On the contrary, for the hard rod fluids, the chain length determines the molecular orientation distribution while the packing fraction has no significant effect on the molecular orientation distribution. When the length of rod is larger than the slit, say, $M = 32$ and 64 in this work, the calculated results indicate that the hard rod molecules always keep the orientation parallel to the surface, which is consistent with the realistic situation. By comparing the molecular orientation of the flexible chains with that of the hard rod fluids, it is found that the molecular stiffness distinctly affects the molecular orientation.

References

[1] Esztermann A, Reich H and Schmidt M 2006 *Phys. Rev.* E **73** 011409

[2] Ye Z C, Cai J, Zhang L S, Liu H L and Hu Y 2005 *Acta Phys. Sin.* **54** 4044 (in Chinese)

[3] Vega C, McBride C and MacDowell L G 2001 *J. Chem. Phys.* **115** 4203

[4] Bolhuis P G, Brader J M and Schmidt M 2003 *J. Phys. Condensed Matter* **15** S3421

[5] Antypov D and Cleaver D J 2003 *Chem. Phys. Lett.* **377** 311

[6] Schmidt M 2001 *Phys. Rev.* E **63** 050201

[7] Sokolova E and Vlasov A 1997 *J. Phys. Condensed Matter* **9** 4089

[8] Bryk P 2003 *Phys. Rev.* E **68** 062501

[9] Chen Y L and Schweizer K S 2002 *J. Chem. Phys.* **117** 1351

[10] Koenderink G H, Vliegenthart G A, Kluijtmans S G, Philipse A P and Lekkerkerker H N W 1999 *Langmuir* **15** 4693

[11] Mao Y, Cates M E and Lekkerkerker H N W 1997 *J. Chem. Phys.* **106** 3721

[12] Cao D P and Wu J Z 2005 *Langmuir* **21** 9786

[13] Yu Y X and Wu J Z 2002 *J. Chem. Phys.* **117** 10156

[14] Roth R, Evans R, Lang A and Kahl G 2002 *J. Phys. Cond. Matter* **14** 12063

[15] Malijevsky A, Bryk P and Sokolowski S 2005 *Phys. Rev.* E **72** 032801

[16] Cao D P and Wu J Z 2005 *Macromolecules* **38** 971

[17] Li Z D, Cao D P and Wu J Z 2005 *J. Chem. Phys.* **122** 174708

[18] Cao D P, Jiang T and Wu J Z 2006 *J. Chem. Phys.* **124** 164904

[19] Cao D P, Zhu M H and Wang W C 2006 *J. Phys. Chem.* B **110** 21882

[20] Bryk P, Bucior K, Sokolowski S and Zukocinski G 2005 *J. Phys. Chem.* B **109** 2977

[21] Cao D P and Wu J Z 2006 *Langmuir* **22** 2712

[22] Patrykiejew A, Pizio O, Sokolowski S and Sokolowska Z 2004 *Phys. Rev.* E **69** 061605

[23] Bryk P, Pizio O and Sokolowski S 2005 *J. Chem. Phys.* **122** 194904

[24] Bryk P and Sokolowski S 2004 *J. Chem. Phys.* **121** 11314

[25] Li Z D, Cao D P and Wu J Z 2005 *J. Chem. Phys.* **122** 224701

[26] Fu D 2006 *J. Chem. Phys.* **124** 164701

[27] Fu D and Li X S 2006 *J. Chem. Phys.* **125** 084716

[28] Cao D P and Wu J Z 2005 *J. Chem. Phys.* **122** 194703

[29] Cao D P and Wu J Z 2004 *J. Chem. Phys.* **121** 4210

[30] Rosenfeld Y 1989 *Phys. Rev. Lett.* **63** 980

[31] Yu Y X, Gao G H and Wang X L 2006 *J. Phys. Chem.* B **110** 14418